

Multiple Invaded Consolidating Materials

A. D. Araújo^{1,2}, J. S. Andrade Jr.^{1,2} and H. J. Herrmann^{1,2}

¹Departamento de Física, Universidade Federal do Ceará, 60451-970 Fortaleza, Ceará, Brazil.

²Institut für Computeranwendungen 1 Universität Stuttgart, 70569 Stuttgart, Germany.

(dated: March 22, 2024)

We study a multiple invasion model to simulate corrosion or intrusion processes. Estimated values for the fractal dimension of the invaded region reveal that the critical exponents vary as function of the generation number G , i.e., with the number of times the invasion process takes place. The averaged mass M of the invaded region decreases with a power-law as a function of G , $M \sim G^{-\alpha}$, where the exponent $\alpha \approx 0.6$. We also find that the fractal dimension of the invaded cluster changes from $d_1 = 1.887 \pm 0.002$ to $d_2 = 1.217 \pm 0.005$. This result confirms that the multiple invasion process follows a continuous transition from one universality class (NTIP) to another (optimal path). In addition, we report extensive numerical simulations that indicate that the mass distribution of avalanches $P(S;L)$ has a power-law behavior and we find that the exponent governing the power-law $P(S;L) \sim S^{-\tau}$ changes continuously as a function of the parameter G . We propose a scaling law for the mass distribution of avalanches for different number of generations G .

PACS numbers: 61.43.Gt, 05.40.-a, 64.60.Ak, 45.70.Ht

I. INTRODUCTION

The veins of gems and ores are often the product of a multiple intrusion of a reacting fluid into a porous soil in which dissolution and subsequent re-crystallization processes are the determining factor. Some examples like porphyry copper deposits [1] or olivine [2] have been studied in the literature and it is known that the surviving network of ore deposits has a fractal structure [3, 4] that can be exploited for mineral exploration [5]. A similar situation can be found in vulcanology when magma is repeatedly injected through the same pathway, each time melting up again the most recent formations to find its way out [6].

The evolution of the pore structure after several invasion-frost-thaw events has been investigated numerically [7], and results indicate that the fractal dimension of invasion clusters varies with the number of invasion cycles. In this work, after invasion takes place, the structure of the porous pathway is randomly healed. In a similar approach [8], an optimized version of the multiple invasion percolation model was studied. Some topological aspects as the acceptance probability and the coordination number were investigated and compared to those of ordinary invasion percolation.

In the cases mentioned [1, 2, 3, 4, 5] above and also in other cases of repeated invasions of corroding, dissolving or melting fluids into a strongly heterogeneous substrate, slowly consolidating matrix fractal patterns are created that reflect the history of the material. It is the aim of this paper to develop a model of multiple invasion in order to simulate how these patterns form and how their fractal dimension changes. In fact, we propose a complete theoretical framework based on scaling laws [6].

The theory of avalanche dynamics has been studied in a variety of contexts, for example in growth models, interface depinning and invasion percolation [9]. The formation of fractal structures, diffusion with anomalous Hurst

exponents and Levy flights, can all be related to the same underlying avalanche dynamics [9]. Normally, the presence of avalanches in the invasion process supposes unchanged porous media. In this work we also investigate the mass-distribution of avalanches and determine how the exponent that characterizes this distribution changes for different cycles of the invasion process. This paper is organized as follows. In Sec. II, we present the model to simulate the multiple invasion in consolidating medium. In Sec. III we show the results for the invaded cluster mass. The results and analysis of the numerical simulation for avalanche distribution are shown in Sec. IV, while the conclusions are presented in Sec. VI.

II. MODEL

In order to simulate the injection process we use the standard non-trapping invasion percolation (NTIP) [10]. In this model the invaded solid is considered to be very heterogeneous and the invading fluid can potentially enter anywhere along the interface. Here the consolidating medium is represented conveniently as a square network. The sites of the lattice can be viewed as the smallest units of constant strength and the randomness of the strength of the medium is incorporated by assigning random numbers to sites. For simplicity, we consider the case in which dissolutions control the fluid invasion.

On our heterogeneous medium we start by applying the standard invasion process of NTIP. For completeness the algorithm is described as follows. Initially, let us assign a random number, p_i drawn from a uniform distribution in the interval $[0;1]$, to each site i of the lattice. We choose one site in the center of the lattice and occupy it. This site represents the injection point of the fluid and is the seed of the invading cluster. We look among the neighboring sites of this cluster (the growth sites) and choose the one which carries the smallest random number. This

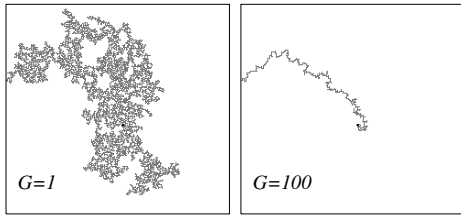


FIG. 1: Typical cluster for different generations on a 256×256 lattice, for $p = 1$. The injection point is localized in the center of the lattice. In figures we show the results for $G = 1$ and 100.

site is then invaded and added to the cluster. Then we increase the list of sites that are eligible to be invaded. At each step of the invasion process, the perimeter of the nearest neighbors of the sites that form the invading cluster is investigated and the site that has the smallest p_i is chosen. This procedure is repeated until the edge of the lattice is reached. At this point the simulation stops and the mass M (i.e., the number of sites belonging to the invaded cluster) of the cluster is computed. The number of sites of the invaded cluster is very often considered as a time parameter.

Now we present the new feature introduced to the standard invasion percolation. After we finish the above described simulation in agreement with customary NTIP, the simulation is performed again starting every time at the same injection point. New random numbers chosen from a uniform distribution in the interval $[0;1]$ are assigned to all sites belonging to the previously invaded cluster before a new invasion process starts. To all other sites, i.e., namely, those that are outside the cluster, we assign a random number homogeneously distributed in the interval $[p; 1]$ where p is a number close to unity. Compared to the support used in the first generation where all sites can be invaded, the second generation appears substantially reduced, because it mostly corresponds to the cluster invaded in the first generation. In this way we generate again an invasion cluster for which $p = 1$ is a subset of the previous one and so necessarily smaller. This procedure is repeated G times, where G is the number of generations. Standard invasion percolation coincides with the case $G = 1$. At each new generation G , the sites of the previous invasion are re-invaded.

Let us first consider the case $p = 1$. In this situation, the invaded cluster is after each time a subset of the previous one so that after a finite number of iterations the cluster does not decrease any longer. The number of generations needed to reach a cluster whose mass remains unchanged depends on the size of the original lattice, because the number of possible available sites is proportional to the system size. Therefore, the saturation number is different for each lattice size. In order to illustrate these changes in the structure after each process of invasion, we show in Fig. 1 typical clusters generated

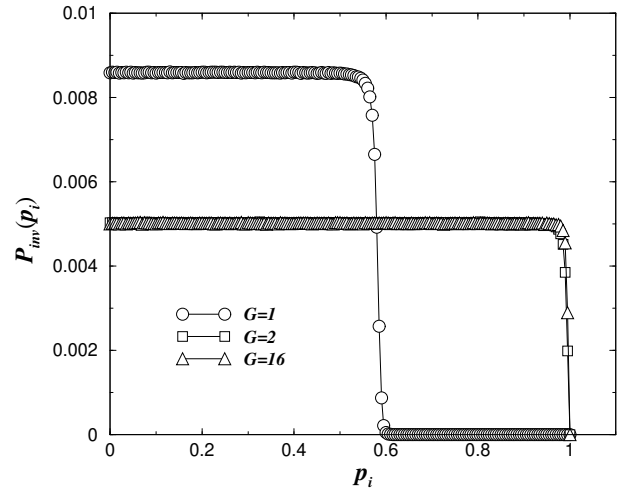


FIG. 2: The probability distribution $P_{\text{inv}}(p)$ of invaded sites for different generations $G = 1$ (circles), 2 (squares) and 16 (triangles), $L = 512$ and $p = 1$.

for a lattice of size $L = 256$ for four different generations G . Another important quantity is the probability distribution of p_i of the invaded sites. In Fig. 2 we present the normalized distribution $P_{\text{inv}}(p)$ for different generations G obtained from 1000 realizations of size $L = 512$. After the completion of the first invasion process, the distribution expectedly displays a transition at $p = p_c$, where p_c is the critical site percolation point, $p_c = 0.59275$ for a square lattice [11]. The same behavior has been observed by numerical simulation in Refs. [7, 8]. For $G = 2$ the distribution $P_{\text{inv}}(p)$ becomes flat and the profile does not change any more as function of G . This happens because when $G > 1$ sites with larger p_i are also invaded.

III. CLUSTER MASS

In our simulations we used the NTIP algorithm for square lattices of sizes $L = 64; 128; 256; 512$ and 1024. For each value of G , we perform simulations for 10000 realizations and compute the mass M_G of the invaded cluster. In Fig. 3, we show the ratio M_G/M_{G-1} as a function of the generation number G . For each size L , G_s is defined as the number of generations at which the mass of the invaded cluster reaches a constant value, i.e., for which $M_{G_s} = M_{G_s-1} = 1$. The results of our simulations shown in Fig. 4 for four values of the generation number G , indicate that the mass M has a power-law dependence on the size L , $M \propto L^{d_g}$, where d_g is the fractal dimension of the invaded cluster. The case $G = 1$ corresponds to the standard invasion percolation model. The value obtained from our simulations, $d_1 = 1.887 \pm 0.002$, is in good agreement with the current estimate $d_1 = 1.8959$ for NTIP [11, 12, 13, 14]. The results shown in Fig. 4

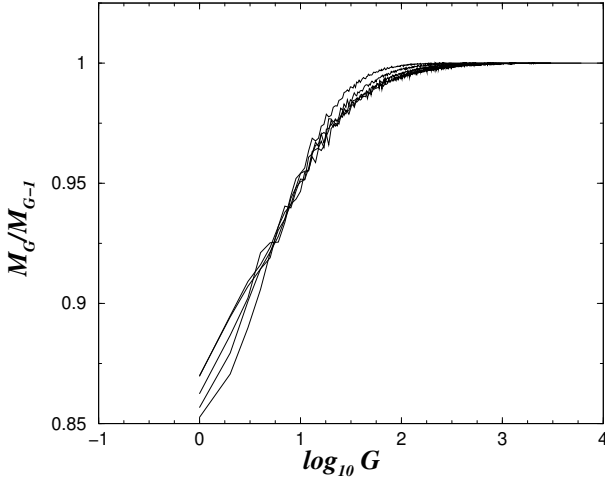


FIG. 3: The evolution of the rate M_G/M_{G-1} as function of the logarithm of the generation number G for $p = 1$. Here M_G is the mass at generation G for different sizes $L = 64; 128; 256$ and 512 .

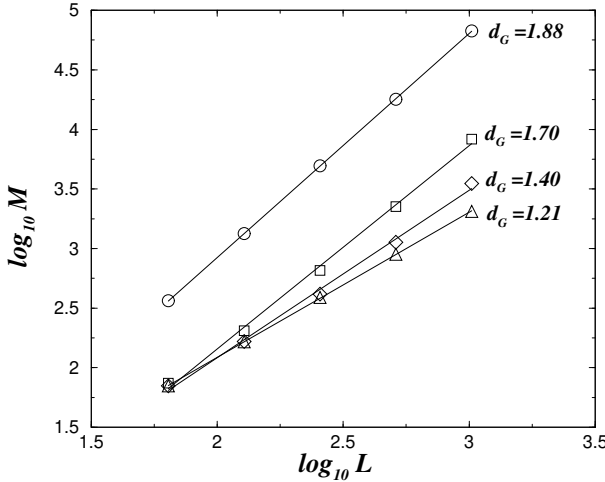


FIG. 4: Log-log plot of the mass M of the invaded cluster versus the system size for different generation numbers $G = 1$ (circles), 100 (squares), 500 (diamonds) and 3000 (triangles), and $p = 1$. The straight lines are best fits to the data and their slopes are the fractal dimensions of the invaded clusters.

indicate that by increasing the generation number the fractal dimension decreases continuously until it reaches a saturation value of $d_s = 1.217 \pm 0.005$ at G_s . This value agrees with the fractal dimension of the optimal path in the strong disorder limit $d_{opt} = 1.22 \pm 0.01$ [15]. As shown in Fig. 5 for large system sizes we find that the average mass of the invaded cluster asymptotically

follows a power-law behavior

$$M \sim G : \quad (1)$$

To better analyze the data, we normalize the mass by the constant M_1 , which is the average mass of the invaded cluster at $G = 1$. Similar to some problems that involve growth surfaces [16], this process has two characteristic regimes: (i) power law evolution and (ii) saturation when $G \gg 1$. To describe this behavior we propose the scaling relation [6]

$$\frac{M(G; L)}{M_1} = L^{-f} \frac{G - N_0}{L^z} : \quad (2)$$

where N_0 is an offset value for the generation number and f and z are scaling exponents. We assume that the scaling function $f(x)$ has the form $f(x) \sim x$ in the limit $x \ll 1$ and $f(x) = \text{const}$ when $x \gg 1$. Furthermore, a direct relation among exponents f , d , and z can be obtained. We find $M \sim M_1 G$ for $L \gg 1$ and, since $M \sim M_1 L$ in the saturation regime ($G \gg 1$), we obtain that $d = d_s - d_1$.

In the crossover region, when the fractal dimension goes from d_1 ($G = 1$) to d_s ($G = G_s$) we have

$$(G - N_0) \sim L^z : \quad (3)$$

From these relations, we obtain that

$$z = -; \quad (4)$$

and from the fact that the fractal dimension has reached the saturation value $d_s = 1.22$, it gives $d = 0.68$. The inset of Fig. 5 shows the data collapse obtained by rescaling $M \sim M_1$ and G according to the scaling form Eq. (2). In this case the best fit to the data gives $d = 0.6$. Substituting into Eq. 4 we find $z = 1.13$.

IV. AVALANCHE DISTRIBUTION

It has been known since a long time that avalanches occur in invasion percolation and that these avalanches obey scaling relations related to percolation theory [17]. An avalanche occurs when a site j is invaded at a value p_j and then a series of sites i connected to this original site are sequentially invaded with $p_i < p_j$. It is also known that the system reaches a self-organized critical state characterized by avalanches of all sizes distributed according to a power law. In the case of NTIP, the exponent corresponding to the power law behavior for the distribution $P(S)$ of avalanche sizes S is $\beta = 1.527$ [17].

In our simulation we found that the exponent corresponding to the case $G = 1$ is $\beta = 1.46 \pm 0.03$. The expected value [17] is outside of our error bars, which we attribute to the fact that we have not reached the asymptotic limit because our systems are too small.

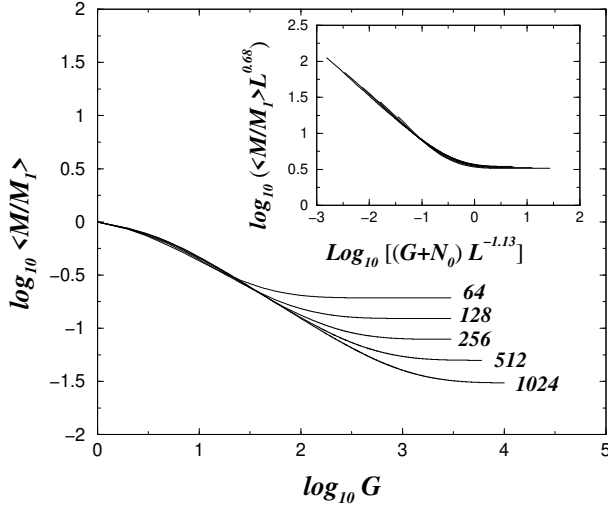


FIG. 5: Log-log plot of the average mass of the invaded cluster M normalized by the mass M_1 of the first invaded cluster, against the number of generations G for different sizes $L = 64; 128; 256; 512$ and 1024 , and $p = 1$. The inset shows the collapse following the scaling relation of Eq. (2).

We performed simulations for different generations G on lattices of sizes $L = 64; 128; 256; 512$ and 1024 , and calculated the size distribution of avalanches. In Fig. 6 we show $P(S)$ for size $L = 512$ and $G = 2; 4; 8; 16; 32; 64$ and 128 . It is clear from this figure that $P(S)$ displays power-law behavior with exponent dependent of the number of generations G . The solid lines indicate the slopes in the two limit cases $G = 1$ (lower) and $G = 128$ (upper).

In Fig. 7, we show how the exponent of the power-law changes as function of the number of generations G . For large values of G the exponent converges to $\tau = 1$. This value is the same found for the distribution of avalanches $P(S)$ in the one-dimensional case [18]. This is consistent with Fig. 1 for $G = 100$ where the avalanche process is limited to a thin path that is essentially an one-dimensional topology.

In Figs. 8 (a) and 8 (b) we show the log-log plot of the distribution of avalanche sizes. It is clear from these figures that $P(S)$ displays a scaling region for intermediate avalanche sizes. In addition the scaling region is followed by a sudden cut-off that decays faster than exponential due to a finite size effect. The range of the power-law region is proportional to the lattice size. As a consequence the biggest avalanches occur in the largest lattice. The position of the cut-off depends on G for fixed L . We propose a scaling form for the mass distribution $P(L; S)$, which accounts for finite size effects and power-law behavior [19]

$$P(S; L) / S \sim f\left(\frac{S}{L}\right); \quad (5)$$

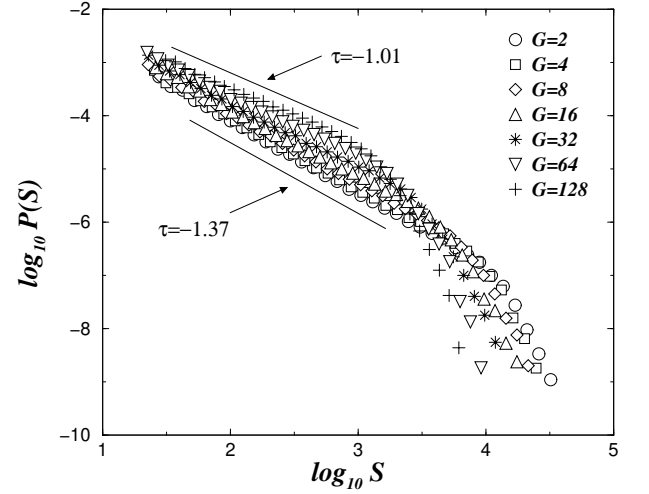


FIG. 6: The mass distribution of avalanches for different generation numbers $G = 2; 4; 8; 16; 32; 64$ and 128 for $L = 512$ and $p = 1$. The slopes of the straight lines follow power-laws with exponent τ . The solid lines indicate the two limit cases $G = 1$ (lower) and $G = 128$ (upper).

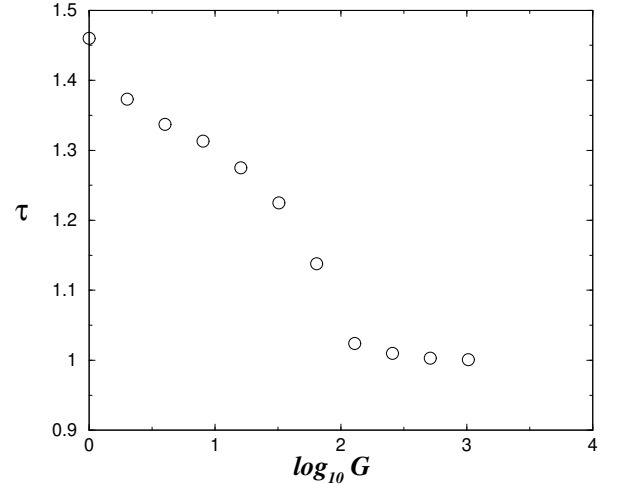


FIG. 7: Log-linear plot of the avalanche exponent τ as function of the generation number G , for $L = 512$ and $p = 1$.

where the function $f(x)$ has a Gaussian form

$$f(x) = \exp[-x^2]; \quad (6)$$

In practice, the appropriate parameters of the scaling function Eq. (5) have been determined here through a nonlinear fitting procedure of the function

$$P(S; L) = A_0 S^{-\tau} \exp[-(S/A_1)^2] \quad (7)$$

to the avalanche data. We observe that both the prefactor A_0 and the crossover amplitude A_1 depend on the

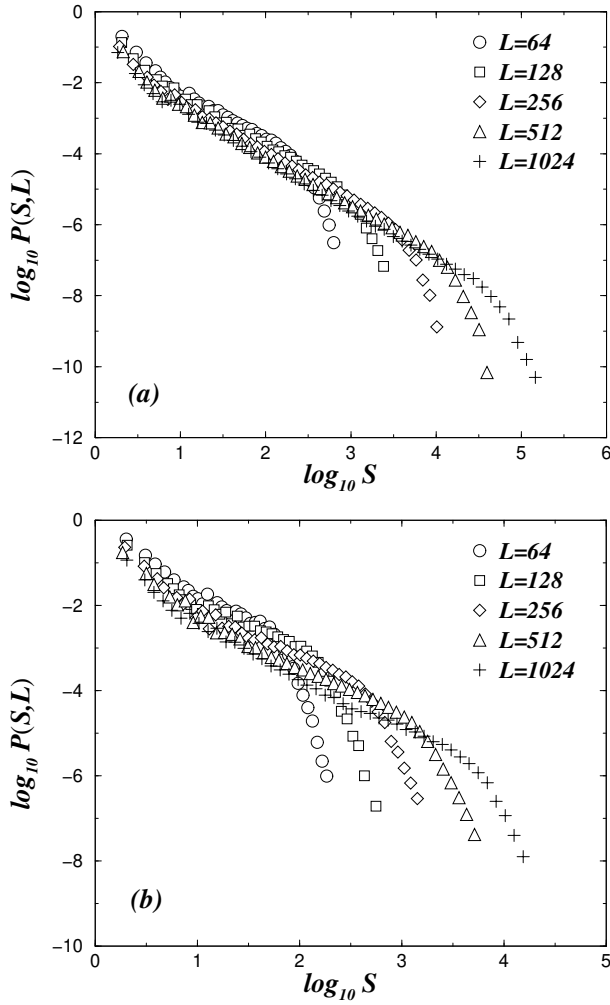


FIG. 8: Log-log plot of the probability distribution of avalanches $P(S;L)$ for various sizes $L = 64; 128; 256; 512$ and 1024 , $p = 1$. (a) $G = 2$ and (b) $G = 128$.

system size.

The solid line in Fig. 9 corresponds to the best fit using Eq. (7) for $G = 2$ and many different sizes L with $\gamma = 1.37$. The inset of Fig. 9 shows the power-law dependence of crossover amplitude on the system size, A_1 / L . The straight lines are the least-squares fits to the data, with the slopes corresponding to the exponent γ in Eq. (5) for different generation numbers.

In Fig. 10 we plot the exponent γ versus G , and see that the exponent has a monotonic behavior as function of the generation number.

In Fig. 11 we show the rescaled function $P(S=L)$ for $G = 16$. The data collapse obtained confirms the validity of the scaling form of Eq. (7). This confirms that the system is self-organized critical and the rescaled distribution shows the asymptotic scaling behavior of Eq. (7).

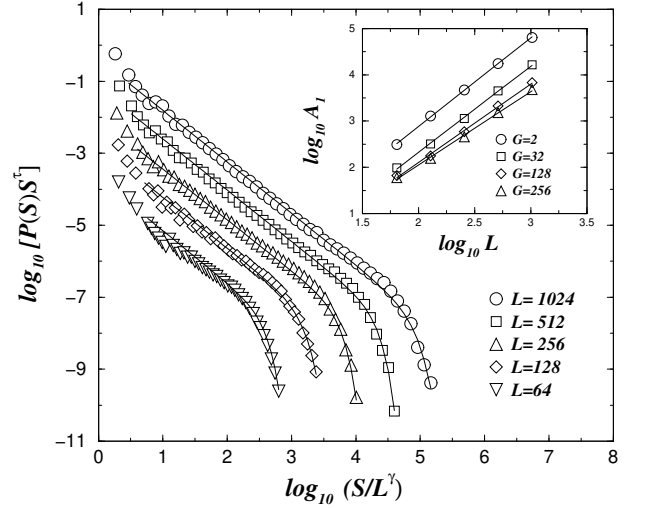


FIG. 9: Log-log plot of the distribution $P(S)$ for $p = 1$ and generation number $G = 2$ for $L = 1024$ (circles), 512 (squares), 256 (up triangles), 128 (diamonds), and 64 (down triangles). The solid lines correspond to the scaling function $y = A_0 S \exp[-(S/A_1)^2]$ with the parameter $\gamma = 1.37$. The inset shows the log-log plot of the crossover amplitude A_1 versus the system size L for $G = 2$ (circles), 32 (squares), 128 (diamonds), and 256 (triangles). The lines are the least-squares fits to the data and the slope is γ .

V. RESULTS FOR $p \neq 1$

In the first part of this work we considered $p = 1$. Now we present simulations for different p very close to unity. In Fig. 12 we show how the mass of the invaded cluster varies as function of the generation number G for a typical realization of the multiply invasion process. In the case $p = 0.9$ the value of the mass shows strong fluctuations. If the probability to occupy sites outside of the previously invaded cluster is raised, the previous invaded region of the porous media is more likely invaded. To understand the qualitative behavior of the invaded cluster as function of the generation G we show in Figs. 13 and 14, typical clusters for two values $p = 0.9$ and $p = 0.999999$, for five different generations $G = 1; 5; 10; 25$ and 50 . For $p = 0.9$, the cluster is more compact and sometimes changes the point where it reaches the border. When $p = 0.999999$, the cluster becomes smaller at each generation.

In order to be more quantitative we calculate the fractal dimension d_f . We measure the mass of the invaded cluster for different generations G for two different probabilities $p = 0.9$ and 0.999999 . Numerical simulations were carried out for 1000 realizations on lattice sizes $L = 64; 128; 256$ and 512 . In Figs. 15 and 16 we present log-log plots of the averaged mass of the invaded cluster versus the lattice size L . The linear fit to the data yields the fractal dimension d_f of the invaded cluster. In the

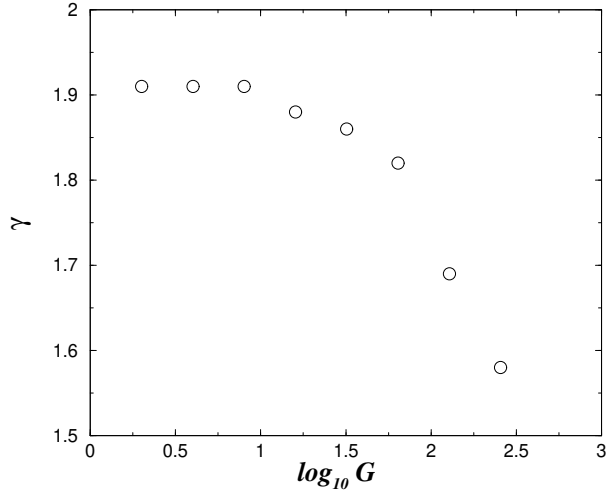


FIG. 10: Log-linear plot of the exponent γ versus the generation number G . $p = 1$.

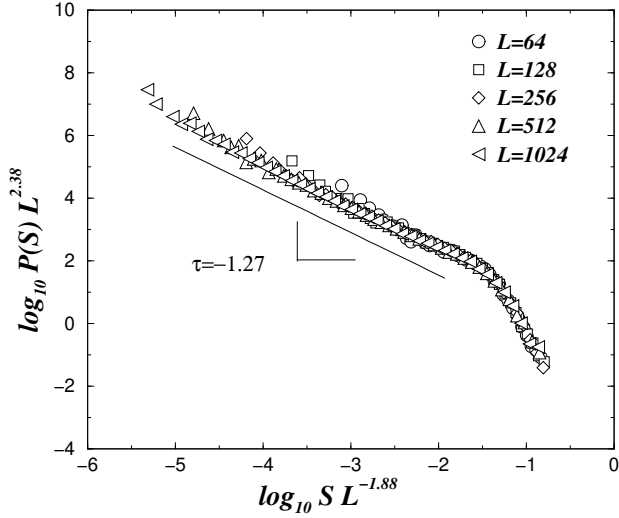


FIG. 11: Log-log plot of the rescaled distribution of avalanche sizes $P(S=L)$ for generation number $G = 16$ and different lattice sizes $L = 64; 128; 256; 512$ and 1204 and $p = 1$.

case $p = 0.9$, the fractal dimension is $d_f = 1.90 \pm 0.01$ for all generations. For $p = 0.999999$ the fractal dimension decreases when G increases. This implies that the fractal dimension of the invaded cluster has a behavior similar to the previously studied case in which $p = 1$.

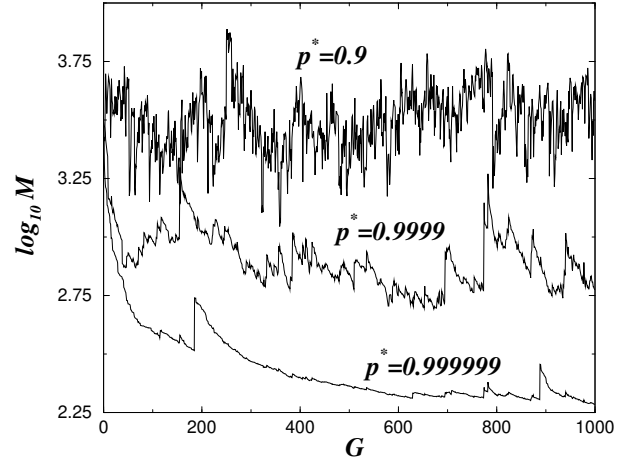


FIG. 12: Linear-log plot of the invaded mass for a typical realization as function of the generation number G , for $L = 512$. From top to bottom, $p = 0.9; 0.9999; 0.999999$.

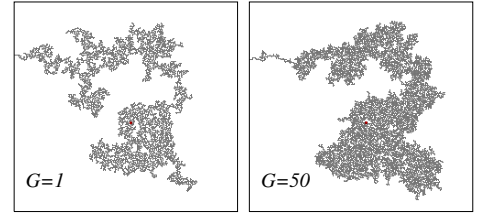


FIG. 13: Typical configurations of invaded clusters at different generations G and $L = 256$. The random number, p_i drawn from a uniform distribution of probabilities in the interval $[p; 1]$ for $p = 0.9$.

VI. CONCLUSIONS

We have presented a comprehensive model to study a multiple invasion process. We have shown that the mass M_G of the invaded cluster decreases with the generation number G . In addition, the fractal dimension

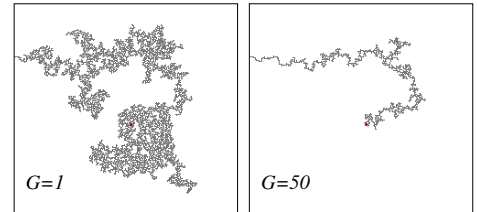


FIG. 14: Typical cluster configurations for invaded clusters at different generations G and $L = 256$. The random number, p_i drawn from a uniform distribution of probabilities in the interval $[p; 1]$ for $p = 0.999999$.

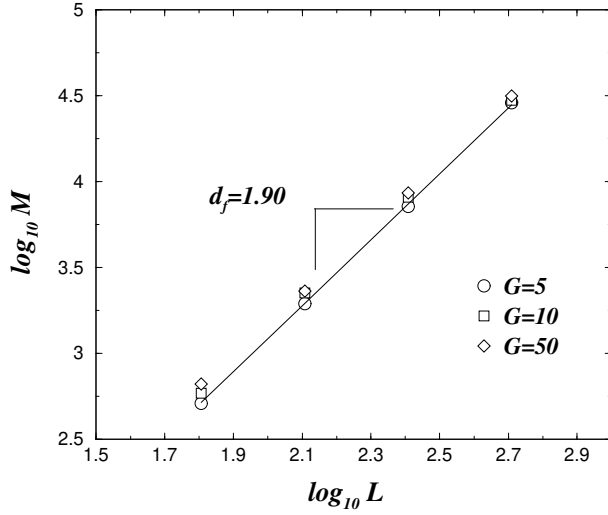


FIG. 15: Log-log plot the averaged mass M as function of the system size L for $p = 0.9$ and $G = 5$ (circles), 10 (squares) and 50 (diamonds). The solid line with slope 1.90 ± 0.01 is the least-square fit to all data sets.

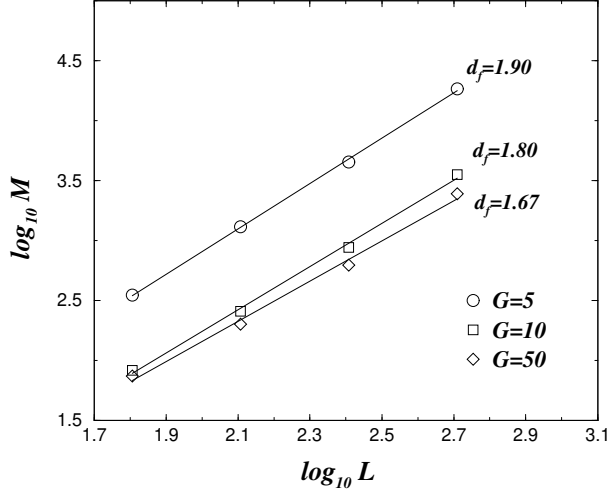


FIG. 16: Log-log plot of the averaged mass M against the system size L for $p = 0.999999$ and $G = 5$ (circles), 10 (squares) and 50 (diamonds). The straight lines are least-square fits to the data, with the numbers corresponding to the fractal dimensions of the clusters.

of the invaded cluster changes from $d_1 = 1.887 \pm 0.002$ to $d_s = 1.217 \pm 0.005$ corresponding to $G = 1$ and $G = G_s$, respectively. This result confirms that the multiple invasion process follows a continuous transition from one universality class (NTIP) to another (optimal path). We confirmed by extensive simulations that the invaded mass follows a power law $M \sim G$ with an exponent 0.6 . In addition the probability distribution of avalanches $P(S; L; G)$ has been studied for different system sizes as function of the parameter G . We found that the mass distribution of avalanches follows a power law where the exponent changes as function of the generation number G . Based on this fact, we suggest that the avalanche process belongs to a different universality class for each G since no crossover scaling seems possible. Our results also indicate that this change in universality class occurs in a continuous way. Concerning the re-invasion of crystallizing, solidifying or healing fluids we conclude that only in the case in which the non-invaded part is not substantially damaged and the healed parts typically do not get much stronger than they were before the invasion, the multiple invasion process converges well to a different universality class, namely that of the optimal path [13]. In the opposite case corresponding to $p \notin 1$, the classical invasion percolation holds for all generations.

VII. ACKNOWLEDGMENTS

We thank CNPq, CAPES, FINEP, FUNCAP, DFG Project 404 and the Max Planck prize for financial support.

-
- [1] M. T. E inandi, Int. Exchange Lecture at Multiple Intrusions, Fluid and Metal Sources, Soc. of Economic Geologists (1994), J. H. D illes and M. T. E inandi, Econ. Geol. 87, 1963-2001 (1992).
 - [2] B. J. W anam aker, T. F. W ong and B. E vans, J. Geophys.

- Res. 95, 15623-15641 (1990).
- [3] D. L. Turcotte, Fractals and Chaos in Geophysics (Cambridge, Univ. Press, 1992).
- [4] C. E. Manning, Geology 22, 335 (1994).
- [5] A. Panabi, Q. Cheng and G. F. Bonhan-Carter, GEEA

- 4, 59 (2004) and references therein.
- [6] E. Luijten, H. W. J. Blote and K. Binder, Phys. Rev. E 56, 6540 (1997)
 - [7] E. Salmon, M. Ausloos and N. Vandewalle, Phys. Rev. E 55, R 6348 (1997)
 - [8] R. A. Zara and R. N. Onody, Int. Mod. Phys. C 10, 227 (1999)
 - [9] M. Paczuski, S. Maslov and P. Bak Phys. Rev. E 53, 414 (1996)
 - [10] D. Wilkinson, J. F. Willemsen, J. Phys. A 16, 3365 (1983).
 - [11] D. Stauffer and A. Aharony, Introduction to Percolation Theory (Taylor Francis, Philadelphia, 1994).
 - [12] J. Feder, Fractals (Plenum Press, New York, 1988).
 - [13] S. Schwarzer, S. Havlin and A. Bunde, Phys. Rev. E 59, 3662 (1999).
 - [14] M. A. Knackstedt, M. Sahimi and A. P. Sheppard, Phys. Rev. E 65, 035101 (R) (2002).
 - [15] M. Cieplak, A. Maritan, and J. R. Banavar, Phys. Rev. Lett. 72, 2320 (1994).
 - [16] A. L. Barabasi and H. E. Stanley, Fractals Concepts in Surface Growth (Cambridge University Press, Cambridge, 1995).
 - [17] S. Roux, E. Guyon, J. Phys. A 22, 3693 (1989).
 - [18] A. M. Alencar, S. V. Buldyrev, A. Majumdar, H. E. Stanley and B. Suki Phys. Rev. E 68, 011909 (2003)
 - [19] J. S. Andrade Jr., S. V. Buldyrev, N. V. Dokholyan, S. Havlin, P. R. King, Y. Lee, G. Paul, and H. E. Stanley, Phys. Rev. E 62, 8270 (2000).